Electronic Supplementary Material (ESI) for Soft Matter.

Photo-induced bond breaking during phase separation kinetics of block copolymer melts: A dissipative particle dynamics study

Ashish Kumar Singh[1], Avinash Chauhan[1], Sanjay Puri[2*], and Awaneesh Singh[1*]

[1]Department of Physics, Indian Institute of Technology (BHU), Varanasi-221005, India.

[2]School of Physical Sciences, Jawaharlal Nehru University, New Delhi-110067, India.

*Emails: awaneesh.phy@iitbhu.ac.in; purijnu@gmail.com

Supplementary Information

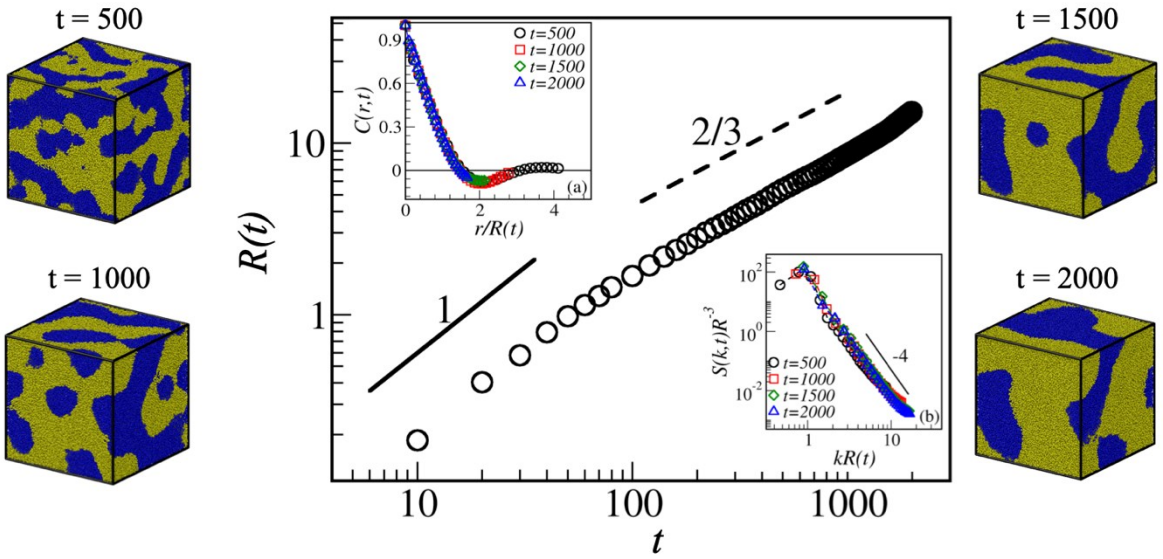

Figure S1: The evolution morphologies, scaling of its characterization functions, and the time dependence of average domain size are depicted for a binary (AB) polymer melt. Our model correctly illustrates the expected growth exponents in the viscous ($\phi = 1$) and inertial ($\phi = 2/3$) hydrodynamic regimes. The excellent data overlap of the correlation function and the structure factor at various times regard the presence of dynamical scaling (see the inset).

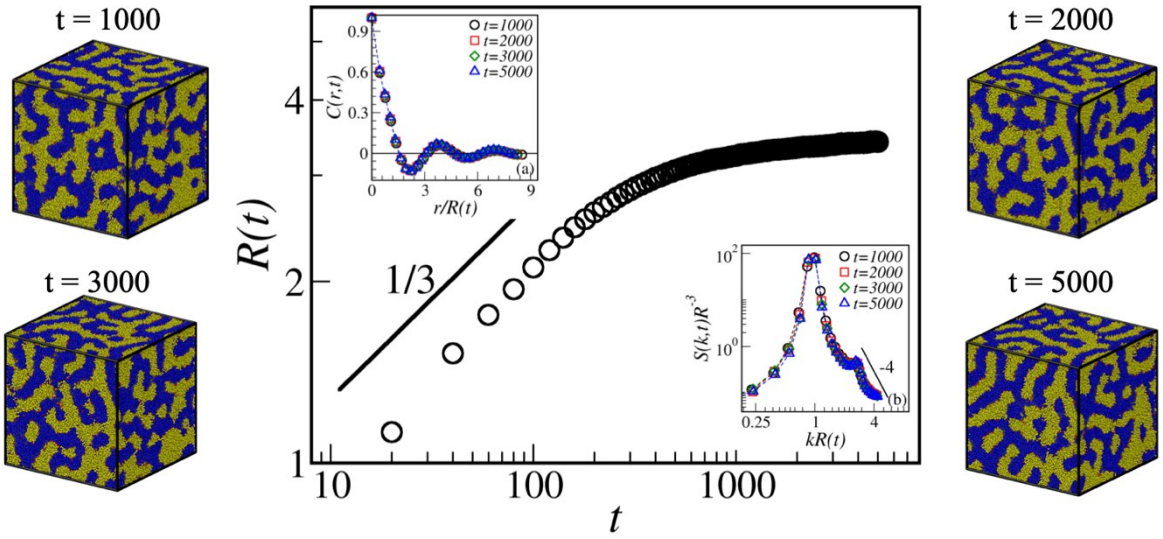

Figure S2: Shows the domain evolution, the scaling of its characterization functions, and the time dependence of the average domain size for BCP melt. Our model correctly illustrates the expected diffusive domain growth ($\phi = 1/3$) for a short while and then saturates to an average length scale. The data overlap of the characteristic functions at various times regard the presence of dynamical scaling (see the inset). The data oscillation around $C(r,t) = 0$, and a secondary peak in $S(k,t)$ confirms the formation of periodic domain structures in microphase separated BCP melt quenched below the critical temperature.

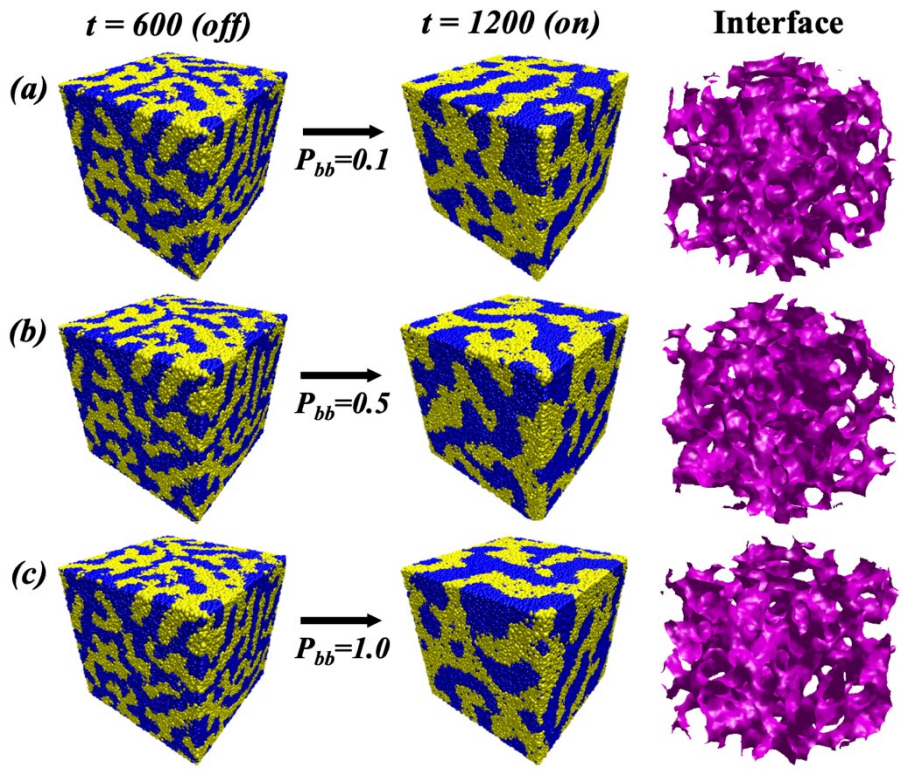

Figure S3: Evolution morphologies of BCP blend after completing off-cycle 1 and on-cycle 2 for set 1 at various bond-breaking probabilities: (a) $P_{bb} = 0.1$, (b) $P_{bb} = 0.5$, and (c) $P_{bb} = 1.0$. The first column shows microphase separated morphology at $t = 600$ as no bond breaking during cycle 1 (off). The second column displays macrophase separated morphology at $t = 1200$ as bonds break during cycle 2 (on) with different P_{bb}; therefore, dissimilar patterns. The third column illustrates the interface evolution between A and B phases for the morphologies shown in the second column.

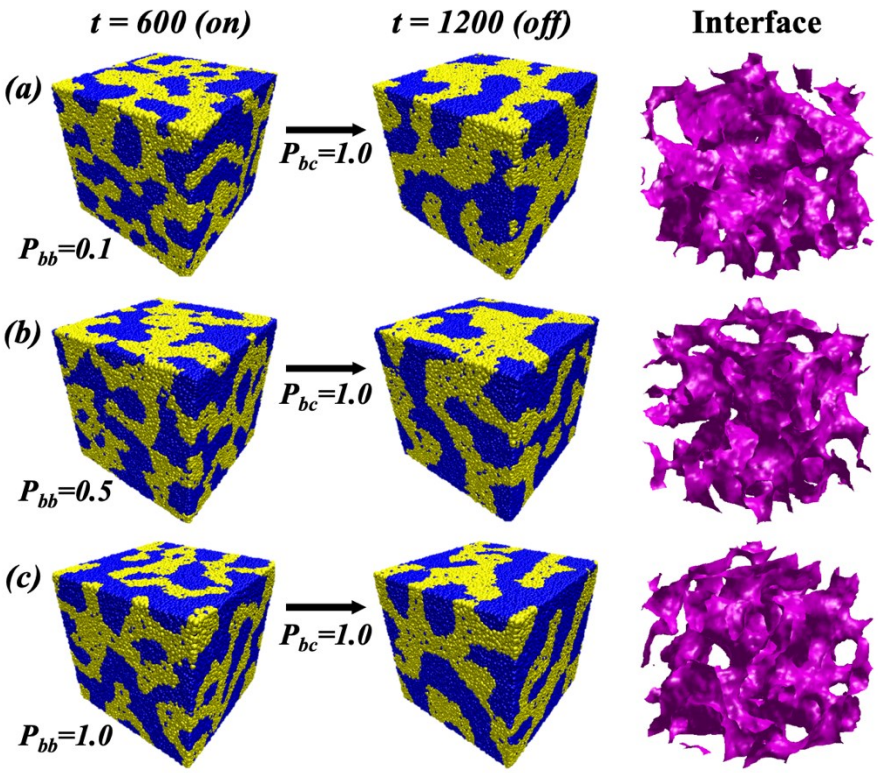

Figure S4: Evolution morphologies of BCP blend for set 2 at the end of on-cycle 1 with various bond-breaking probabilities: (a) $P_{bb} = 0.1$, (b) $P_{bb} = 0.5$, and (c) $P_{bb} = 1.0$., and at the end of off-cycle 2 with a bond combination probability, $P_{bc} = 1.0$. The first column shows macrophase separated morphology at $t = 600$ due to bond breaking through cycle 1 (on) with diverse P_{bb}; thus, varied patterns. The second column displays microphase separated morphologies at $t = 1200$ during cycle 2 (off) when bonds recombine with a probability, P_{bc}; different patterns as the domain formed during cycle 1 for each P_{bb} is dissimilar. The third column illustrates the interfaces for morphologies shown in the second column.

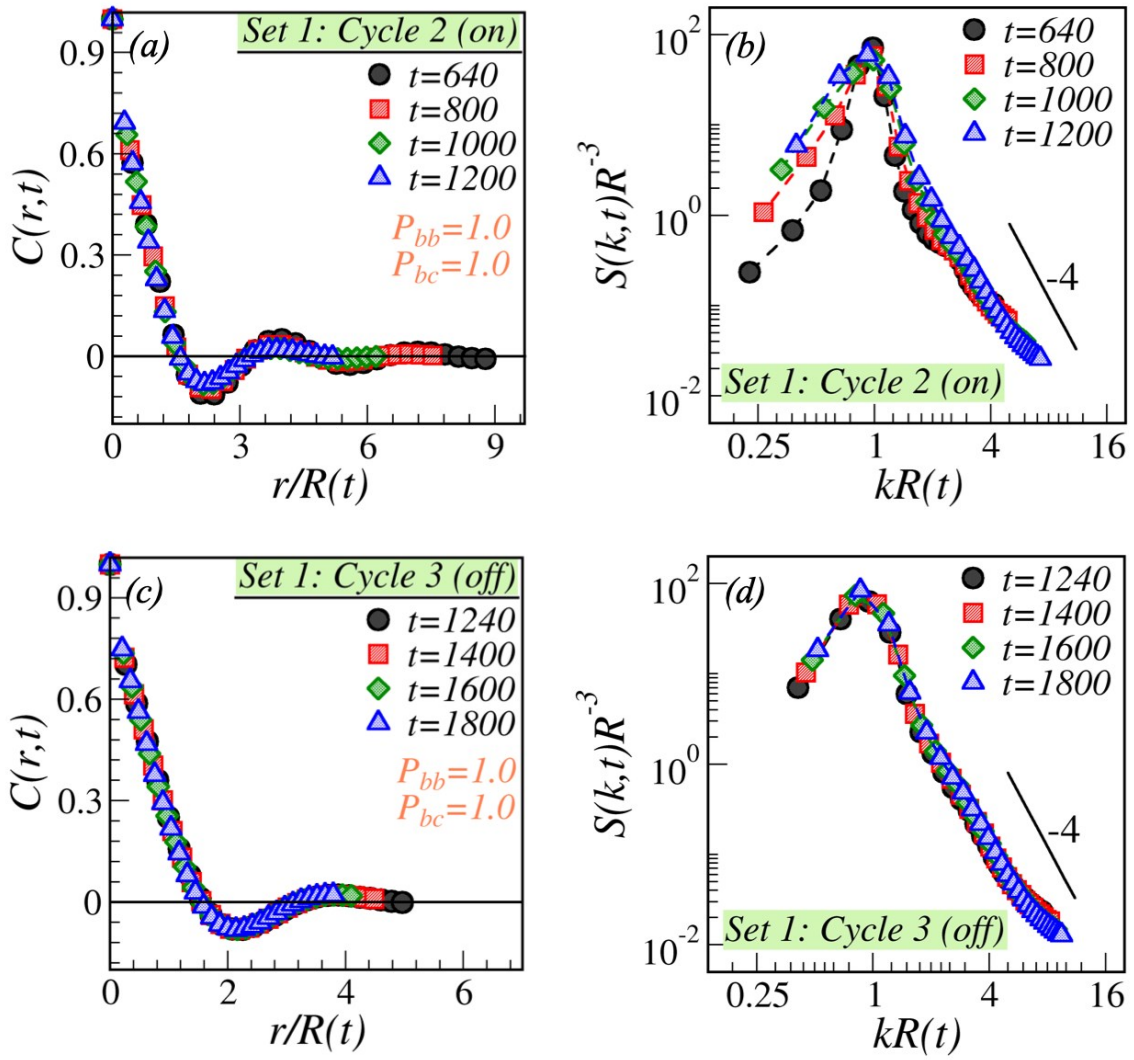

Figure S5: (a-b) Scaling of the correlation function ($C(r,t)$ vs. $r/R(t)$) and the structure factor ($S(k,t)R(t)^{-3}$ vs. $kR(t)$) for the evolution through cycle 2 (bond breaking on) for set 1. The system shows a small deviation from the scaling for early times (black and red curves at $t = 640$ and $t = 800$, respectively) when the kinetics is typically chemically controlled (bond breaking). However, we noted an excellent scaling in the system at late times (green and blue curves at $t = 1000$ and $t = 1200$, respectively). (c-d) We plot $C(r,t)$ vs. $r/R(t)$ and $S(k,t)R(t)^{-3}$ vs. $kR(t)$ for the evolution through cycle 3 (bonds are recombining) for the same set as in (a-b). The data overlap at various times reveals an excellent scaling in the system. The bond-breaking probability is set to $P_{bb} = 1.0$ during on cycles, and bond combination probability is set to $P_{bc} = 1.0$ during off periods. Each data set is averaged over five ensembles. A solid line with slope -4 signifies the Porod's law, *i.e.*, $S(k,t) \sim k^{-4}$ for $k \to \infty$.

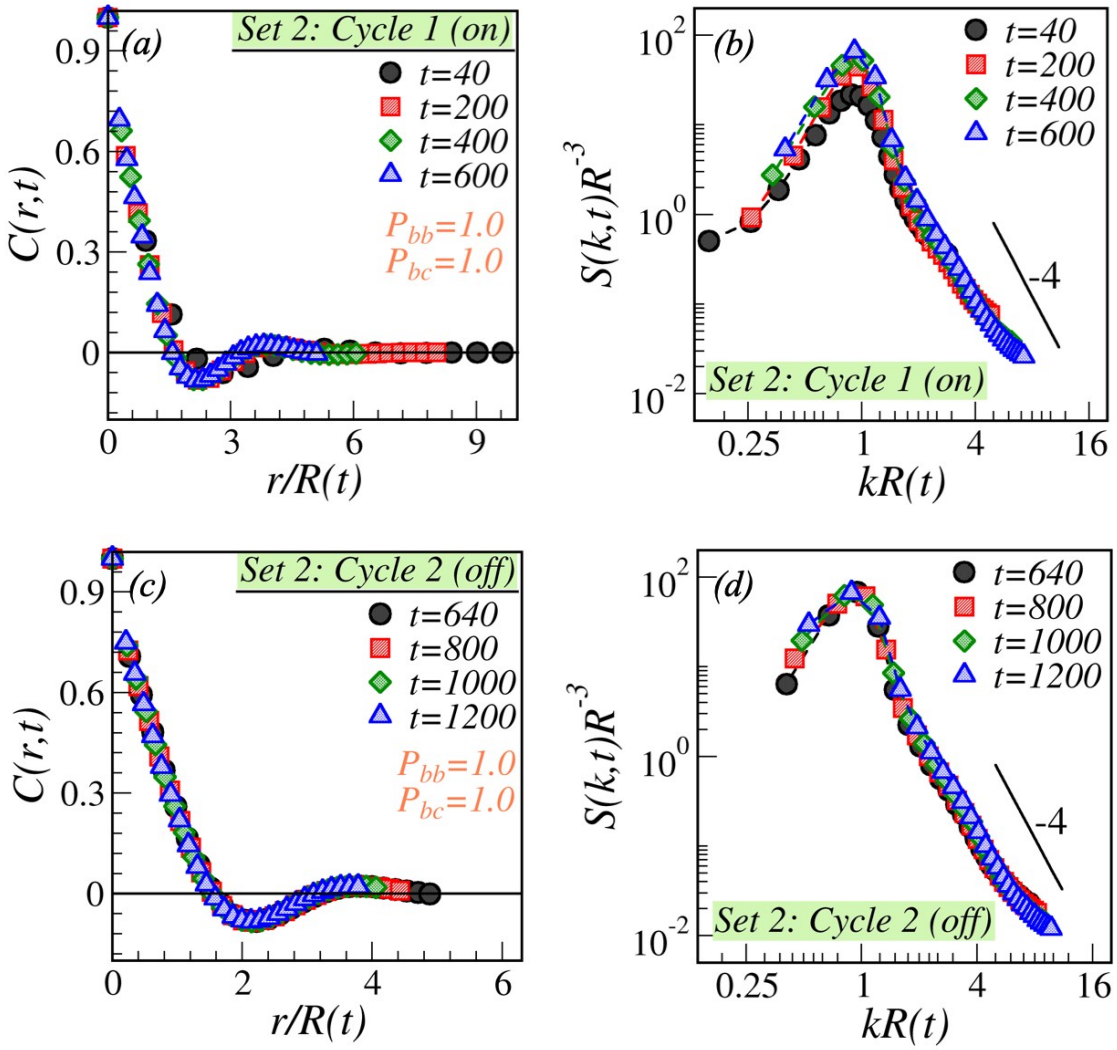

Figure S6: (a-b) We plot the correlation function ($C(r,t)$ vs. $r/R(t)$) and the structure factor ($S(k,t)R(t)^{-3}$ vs. $kR(t)$) for the evolution through cycle 1 (bond breaking on) for the set 2. Similar to the first on-cycle in set 1, a small deviation from the scaling is observed at early times (black and red curves at $t = 40$ and $t = 200$, respectively) for the chemically controlled regime. However, we note an excellent scaling at late times (green and blue curves at $t = 400$ and $t = 600$, respectively). (c-d) The plots $C(r,t)$ vs. $r/R(t)$ and $S(k,t)R(t)^{-3}$ vs. $kR(t)$ for the evolution through cycle 2 (bonds are recombining) for the same set as in (a-b) reveal an excellent scaling in the system. The bond-breaking probability is set to $P_{bb} = 1.0$ during on cycles, and bond combination probability is set to $P_{bc} = 1.0$ during off cycles. Each data set is averaged over five ensembles.

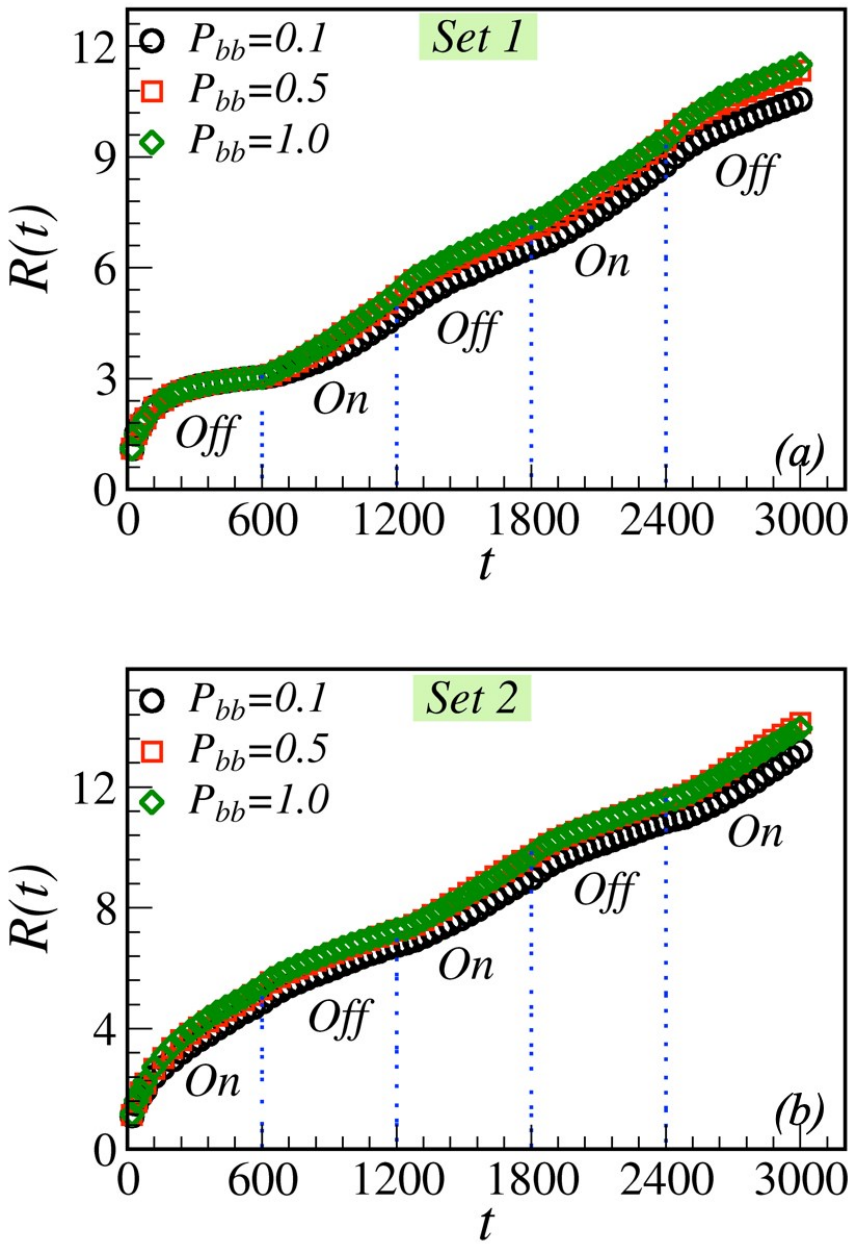

Figure S7: Time dependence of the average domain size for the set 1 is shown in (a) and for the set 2 is exhibited in (b) for the different cases represented by the various symbol types.